

Effect of $\text{Fe}_x\text{Ca}_y\text{CO}_3$ and CaCO_3 Scales on the CO_2 Corrosion of Mild Steel

Hamed Mansoori,^{†,*} Bruce Brown,^{*} David Young,^{*} Srdjan Nešić,^{*} and Marc Singer^{*}

Calcium ions are usually present at high concentrations in brines produced with oil and gas. Such brines are typically saturated with respect to CaCO_3 . Consequently, precipitation of CaCO_3 as scale on the internal wall of the pipeline can readily occur due to changes in operational and environmental parameters as produced fluids are transferred from downhole to surface facilities. Despite its importance, there is minimal research in the literature addressing the effect of calcium ions, and specifically CaCO_3 scale, on the CO_2 corrosion mechanism. The main objectives of this research are to further broaden the mechanistic understanding of CO_2 corrosion of mild steel in the presence of high concentrations of calcium ions and evaluate the protectiveness that $\text{Fe}_x\text{Ca}_y\text{CO}_3$ and CaCO_3 scale confers against further corrosion. The corrosion behavior was studied *in situ* by electrochemical methods, including linear polarization resistance and open-circuit potential, along with weight loss using a UNS G10180 steel with ferritic-pearlitic microstructure. Surface characterization of the scale and corrosion product was performed using scanning electron microscopy, energy dispersive x-ray spectroscopy, and x-ray diffraction. A descriptive model is proposed for the CO_2 corrosion mechanism of mild steel in the presence of high concentrations of calcium ions. Unprotective $\text{Fe}_x\text{Ca}_y\text{CO}_3$ ($y > x$) and CaCO_3 scales were observed to act as a mass transfer barrier that could promote surface conditions favoring FeCO_3 precipitation. The presence of uniform CaCO_3 scale did not result in the onset of localized corrosion at the conducted experimental conditions.

KEY WORDS: CaCO_3 , CO_2 corrosion, corrosion mechanism, FeCO_3 , $\text{Fe}_x\text{Ca}_y\text{CO}_3$, mild steel

INTRODUCTION

Over the past decades, mechanisms of CO_2 corrosion of mild steel and the protective properties of its corrosion products have been intensively studied and documented by different researchers.¹⁻¹¹ However, most of these studies have been performed in various dilute solutions of sodium chloride (NaCl), while, in reality, calcium ions are also present in brines associated with geologic formations.¹²⁻¹⁵ CaCO_3 (as mineralogically named calcite) and FeCO_3 (siderite) are isostructural with a hexagonal unit cell.¹⁶ This indicates that their constituent cations (Ca^{2+} and Fe^{2+}) can coexist in a substitutional mixed carbonate, designated with the formula $\text{Fe}_x\text{Ca}_y\text{CO}_3$ ($x + y = 1$). The solubility of CaCO_3 in water is about two orders of magnitude greater than the solubility of FeCO_3 . Therefore, the substitution of Fe^{2+} by Ca^{2+} in the lattice of FeCO_3 can be hypothesized to increase the solubility of the mixed carbonate layers in comparison with pure FeCO_3 layers. In addition to changing the solubility of FeCO_3 , compositional heterogeneity, and morphological alteration are expected when Ca^{2+} incorporates into the FeCO_3 crystal structure. This strongly suggests that the presence of Ca^{2+} in the solution and possible precipitation of a mixed $\text{Fe}_x\text{Ca}_y\text{CO}_3$ and/or CaCO_3 scale on the steel surface would influence the CO_2 corrosion mechanisms.

There are only a handful of studies in the literature that address the effect of $\text{Fe}_x\text{Ca}_y\text{CO}_3$ and/or CaCO_3 scale on CO_2 corrosion.¹⁷⁻²⁵ Such studies usually relied on the initial Ca^{2+} concentration rather than the CaCO_3 saturation degree of the bulk solution as the core influential parameter. In addition, the flow

characteristics of the experimental setups were typically not well-defined, rendering the results difficult to reproduce.¹⁶ When a solution is initially supersaturated with respect to CaCO_3 ($S_{\text{CaCO}_3} > 1$), precipitation of CaCO_3 is inevitable due to its fast kinetics, particularly at elevated temperatures. Once precipitation starts, the aqueous solution tends toward an equilibrium state with a saturation in CaCO_3 close to unity ($S_{\text{CaCO}_3} \approx 1$). This can lead to significant changes in water chemistry (different pH, $[\text{Ca}^{2+}]$, etc.) between the initial (before precipitation) and the final (after precipitation) conditions. The reason why the results of such studies, which are supposed to be comparable, often appear contradictory can be traced back to poorly controlled water chemistry and different flow conditions accompanied with misleading analysis.¹⁶ These discrepancies invite the development of a systematic and well-designed procedure for elucidating the relevant issues surrounding CO_2 corrosion in the presence of Ca^{2+} ions.

In the study, the protectiveness of mixed $\text{Fe}_x\text{Ca}_y\text{CO}_3$ and pure CaCO_3 scale in CO_2 corrosion are investigated in two separate experimental scenarios.

1. The first scenario is related to the evaluation of mixed $\text{Fe}_x\text{Ca}_y\text{CO}_3$. The electrolyte is saturated with respect to CaCO_3 ($S_{\text{CaCO}_3} = 1$). In this scenario, bulk precipitation of CaCO_3 would not occur. However, the formation of a mixed $\text{Fe}_x\text{Ca}_y\text{CO}_3$ is expected due to a favorable water chemistry achieved on the steel substrate during the corrosion process.
2. The second scenario is related to the evaluation of pure CaCO_3 . The electrolyte is initially supersaturated with

Submitted for publication: June 5, 2019. Revised and accepted: September 18, 2019. Preprint available online: September 18, 2019, <https://doi.org/10.5006/3290>.

[†] Corresponding author. E-mail: hm419213@ohio.edu.

^{*} Institute for Corrosion and Multiphase Technology, Department of Chemical & Biomolecular Engineering, Ohio University 342 West State Street, Athens, Ohio, 45701.

respect to CaCO_3 , $S_{\text{CaCO}_3} > 1$, leading to rapid precipitation of a CaCO_3 scale on a steel surface, followed by a unity saturation with respect to CaCO_3 .

Tavares, et al., performed one of the rare CO_2 corrosion studies on carbon steel where the solution was saturated with respect to CaCO_3 over the course of experiments, achieved by adding bulk CaCO_3 to the test solution.²⁶ For comparison, this study would correspond to the first scenario presented above. The authors reported that general corrosion was predominant rather than pitting corrosion. Moreover, they observed a decline in the corrosion rate over time (28 d) as determined by weight loss (WL). The authors also reported that the average corrosion rate for mild steel in the CaCO_3 -saturated solution was lower than when the solution was free from dissolved CaCO_3 . In fact, this could be due to a different initial pH of the two solutions (pH 2.7 without presence of CaCO_3 and pH 4.4 with CaCO_3) rather than a direct effect of Ca^{2+} ions on surface layer protectiveness against corrosion. Mansoori, et al., have recently investigated the first scenario in conditions where the water chemistry (pH, Fe^{2+} concentration) of the test solutions was tightly maintained over the course of long-term experiments and the mass transfer conditions of the experimental setup were well-defined.²⁷ They reported that in a CaCO_3 -saturated solution ($[\text{Ca}^{2+}] \approx 160$ ppm, $[\text{Fe}^{2+}] \approx 10$ ppm, solution pH maintained at 6.2, solution ionic strength 0.18 M), a mixed iron-calcium carbonate formed on the steel surface, with a mole fraction of iron higher than calcium. It was concluded that such iron-calcium carbonate scale was as protective as FeCO_3 . Because the corrosion behavior of mild steel in the presence of Ca^{2+} highly depends on the characteristics of the surface layers, there is a further need to investigate the first scenario in harsher conditions as seen in oilfield brines; for example, at higher calcium concentrations, higher ionic strength, and lower pH.

To the authors' best knowledge, there is limited experimental data related to the second scenario. Bekhrad and Javidi, have conducted electrochemical experiments to evaluate general and localized corrosion of carbon steel covered with CaCO_3 scale in CO_2 environments.²⁸ The API 5L X52 specimen was covered with a CaCO_3 scale layer precipitated from a separate supersaturated solution and then transferred to the main corrosion test cell which did not contain any dissolved Ca^{2+} . They concluded that the presence of CaCO_3 scale on the carbon steel resulted in lowering the general corrosion rate and did not promote localized corrosion on the specimens. However, in oilfield pipelines, after precipitation of CaCO_3 scale from a supersaturated condition, the brine would still contain dissolved Ca^{2+} (now in unity saturation with respect to CaCO_3). Although the work by Bekhrad and Javidi is one of the few relevant and comprehensive works to evaluate protectiveness of CaCO_3 scale, the used methodology did not resemble oilfield conditions as the CO_2 corrosion experiment with the "calcite-covered carbon steel" was performed in the absence of dissolved Ca^{2+} .

There has been other research performed in the context of external corrosion of buried pipelines, under cathodic protection, where CaCO_3 scale precipitated on the steel from soils rich with calcium ions. For example, Ghanbari and Lillard conducted experiments to evaluate the effect of CaCO_3 scale formation on alternating current (AC) induced corrosion of X65 carbon steel at atmospheric pressure (open air) and room temperature.²⁹ They concluded that CaCO_3 deposits did not have any effect on AC corrosion rates other than by decreasing the exposed surface area of the steel. The experimental

conditions of these tests were designed to add more understanding to the influence of external AC corrosion of a carbon steel pipeline under cathodic protection and in CaCO_3 scaling conditions. With so few references available that address the influence of pure CaCO_3 scale on CO_2 corrosion mechanisms, a true gap in the knowledge related to the internal corrosion of oil and gas pipelines has been identified.

The main objectives of the current research are to further broaden the mechanistic understanding of CO_2 corrosion of mild steel in the presence of high concentrations of Ca^{2+} . This is achieved by evaluating:

- Protectiveness of mixed iron-calcium carbonate layers obtained while the test solution is saturated with respect to CaCO_3 (referred as the first scenario).
- Protectiveness of pure CaCO_3 scale formed in simulated CaCO_3 supersaturated conditions, while avoiding FeCO_3 precipitation (referred as the second scenario).

EXPERIMENTAL SETUP

Figure 1 depicts the 4-L experimental setup used to conduct the corrosion studies in this paper. This apparatus is equipped with an impeller to create uniform mass transfer characteristics and uniform wall shear stress across the specimen surfaces. It includes stationary specimen holders with seals to eliminate oxygen contamination of the experimental setup during specimen retrieval from the test solution for surface analysis, as shown in Figure 1. In this setup, all corrosion specimens (including WL, surface analysis, and electrochemical measurements) experience identical flow characteristics (mass transfer rate and shear stress). The specimens are identical in size and are held in place by specimen holders located at the same radial distance from the center of the glass cell. The flow and mass transfer characteristics of this experimental setup have been reported in a recent publication by the authors.²⁷

METHODOLOGY

Two series of experiments were conducted (and repeated) to investigate the protectiveness of $\text{Fe}_x\text{Ca}_y\text{CO}_3$ formed in solutions with high concentrations of Ca^{2+} , in CO_2 corrosion (first scenario). One set of experiments was performed in CaCO_3 -saturated solution ($[\text{Ca}^{2+}] \approx 6,000$ ppm) and one without Ca^{2+} (baseline experiment); other than that, both test series were conducted under the same conditions based on the test matrix presented in Table 1. The solutions, with and without Ca^{2+} , contained 1 wt% NaCl in the presence of 0.53 bar (53 kPa) pCO_2 at 80°C (1 bar [100 kPa] total pressure of the glass cell). An excess amount of powdered CaCO_3 reagent (15 g/L) was initially added to the solution in order to keep it saturated with respect to CaCO_3 over the course of the 7-d experiments. After adding CaCO_3 , the pH was adjusted to a value of 5.50 with 1.0 M HCl. For the tests without CaCO_3 , the pH was adjusted to 5.50 by adding NaHCO_3 to the solution. For the experiments conducted in the absence of Ca^{2+} , sodium perchlorate salt (NaClO_4) was used to achieve the same ionic strength as the experiment with the presence of Ca^{2+} . NaClO_4 is highly soluble in water and has been used to adjust ionic strength as it does not react with common anions and cations.³⁰ Although the authors do not attribute any specific effect of Cl^- on the corrosion processes presented in this paper, many literature works have linked the presence of chloride ions with enhanced localized corrosion³¹⁻³³ and adsorption properties.³⁴⁻³⁶ No such

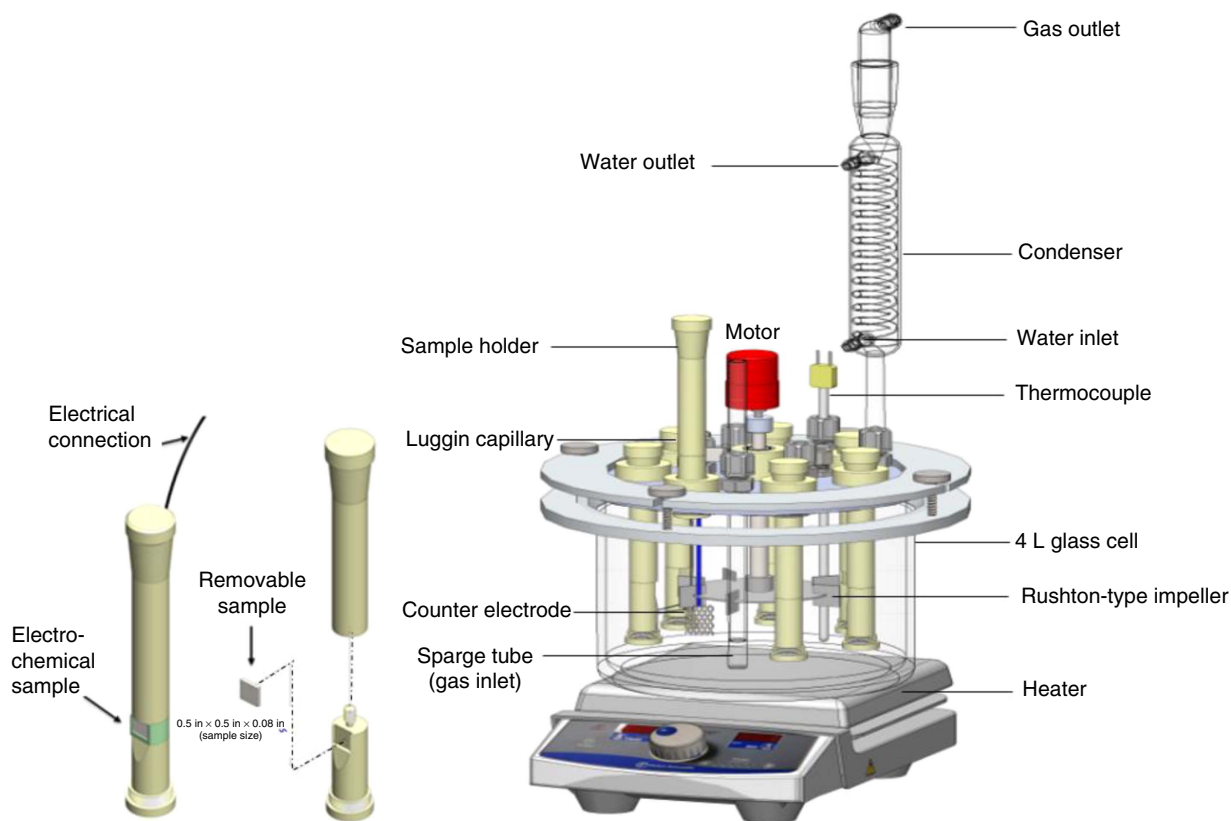


FIGURE 1. Schematic of experimental setup equipped with impeller, capable of ensuring uniform mass transfer across specimen surfaces and with removable specimen holders (drawing courtesy of Cody Shafer, OU ICMT).

Table 1. Experimental Conditions Used to Evaluate Protectiveness of $Fe_xCa_yCO_3$ (First Scenario)

Parameter	Description	
	Without $CaCO_3$	With $CaCO_3$
Specimen steel	UNS G10180 with ferritic-pearlitic microstructure, flat square specimen ($A = 1.5 \text{ cm}^2$)	
Temperature	80°C	
pCO_2	0.53 bar	
pH	5.5±0.2 (adjusted by $NaHCO_3$)	5.5±0.1 (adjusted by HCl)
Electrolyte	1 wt% $NaCl+NaHCO_3+NaClO_4$ (ionic strength= 0.6 M)	1 wt% $NaCl+HCl+CaCO_3$ (ionic strength = 0.6 M)
$CaCO_3$ saturation degree (S_{CaCO_3})	0	Unity ($[Ca^{2+}] \approx 6,000 \text{ ppm}$)
$FeCO_3$ saturation degree (S_{FeCO_3})	0 (initial) to 10.8 (final)	0 (initial) to 1.2 (final)
Dissolved O_2	<5 ppb	
Reference electrode	Saturated Ag/AgCl	
Impeller rotation speed	20 rpm	
Mass transfer conditions	Equivalent to 0.5 m/s in a 0.1 m ID pipe	
Electrochemical techniques	OCP, LPR, EIS	
Surface analysis techniques	XRD, SEM/EDS	
Experiment duration	7 d	

characteristics have been reported about $NaClO_4$ and because $NaClO_4$ does not yield free Cl^- when it dissociates in water, the two series of experiments had the same Cl^- concentration while maintaining identical ionic strength of 0.60 M. By this

approach, any observed difference in the experimental results would be due to the change in calcium concentration and would not be related to a change in chloride ions concentration. The solutions were deoxygenated by sparging with CO_2 for 2 h

Table 2. Experimental Conditions Used to Evaluate Protectiveness of CaCO₃ Scale (Second Scenario)

Parameter	Description
Temperature	80°C
pCO ₂	0.53 bar
pH	5.5±0.1
Electrolyte	1 wt% NaCl+HCl+CaCO ₃ (ionic strength = 0.6 M)
CaCO ₃ saturation degree in bulk solution	unity (6,000 ppm Ca ²⁺)
Impeller rotation speed	20 rpm
Mass transfer conditions	equivalent to 0.5 m/s in a 0.1 m ID pipe
Specimen steel	UNS G10180
Cathodic polarization potential	-200 mV _{OCP}
Methods for monitoring corrosion behavior	LPR, OCP
Dissolved O ₂	<5 ppb
Cathodic protection duration (formation of CaCO ₃)	5 d
Prescaled (CaCO ₃) specimen exposed for active corrosion	7 d

prior to insertion of the specimens. The oxygen content of the outlet gas was measured at 80°C (after introducing the specimens) using an Orbisphere 410[†] sensor. The oxygen concentration was lower than 5 ppb throughout the experiments. CO₂ gas was continuously bubbled into solution to maintain CO₂ saturation during the 7-d corrosion experiments.

The square-shape specimens had dimensions of 12.3 mm × 12.3 mm × 2.5 mm. The four side edges and one face of the WL specimens were coated with a thin layer of xylene epoxy (Whitford^{TM†}) before immersion in the test solutions. Therefore, the exposed surface area of such specimens was 1.5 cm². An electrical wire was soldered to the electrochemical specimen and then was embedded in waterproof epoxy resins (MarineWeld^{TM†}) and left overnight for solidification process (with an exposed surface area of 1.5 cm²). A schematic of WL and electrochemical sample (specimen) is shown in Figure 1. The electrochemical and WL specimens were then polished with silicon carbide abrasive papers up to 600 grit and rinsed with isopropanol. Following the polishing process, the specimens were rinsed with isopropanol and placed in an ultrasonic cleaner for 2 min. Finally, they were dried by cold air and ready for immersion. A three-electrode system (working, counter, and reference electrodes) and Gamry Reference600^{TM†} potentiostat were used to conduct in situ electrochemical measurements. A platinum-coated titanium mesh with a dimension of 20 mm × 30 mm × 1 mm was used as the counter electrode and saturated Ag/AgCl was used as the reference electrode. Ferrous iron (Fe²⁺) concentration was measured twice daily by spectrophotometry using phenanthroline as the reagent.³⁷ The rotational speed of the impeller was set at 20 rpm, which provided a mass transfer rate similar to one obtained for example in 0.1 m inner diameter (ID) pipe flow at a velocity of 0.5 m/s (the mass transfer characterization of the experimental setup is provided in a previous publication²⁷). The corrosion rate was measured at least twice per day using linear polarization resistance (LPR); open-circuit potential (OCP) was also recorded. Solution resistance, used for adjusting the polarization resistance of the working electrode, was measured by the electrochemical impedance spectroscopy (EIS) technique after each LPR reading. Two specimens were retrieved

from the glass cell at days 2, 4, and 7 from each experiment to obtain WL and conduct surface characterization using scanning electron microscopy/energy dispersive x-ray spectroscopy (SEM/EDS) and x-ray diffraction (XRD).

The second scenario explained above investigates the protectiveness of CaCO₃ scale precipitated from a supersaturated condition with respect to CaCO₃. While the properties of "pure" FeCO₃ layers have been extensively investigated,³⁸⁻³⁹ this is not the case for "pure" CaCO₃. The protectiveness of CaCO₃ has not systematically been studied as it is difficult to promote CaCO₃ precipitation while, at the same time, suppressing FeCO₃ formation. However, the current research was successfully performed using a novel methodology. The idea was to precipitate a uniform CaCO₃ layer on the steel substrate, without the participation of Fe²⁺ (coming from the corroding steel) in the carbonate formation process. To reach this goal, the working electrodes were cathodically polarized (-200 mV_{OCP}) for 5 d. Table 2 shows the experimental conditions used for this series of experiments. The corrosion rate was reduced significantly by cathodic polarization, hence, minimizing dramatically the Fe²⁺ production (the Fe²⁺ concentration was so low that it was not detectable in the bulk solution by spectrophotometry). The bulk solution was kept saturated with respect to CaCO₃ by introducing an excess amount of powdered CaCO₃ to the solution at the beginning of the experiments. The experimental conditions used for this series of experiments were identical to those for the first scenario corrosion experiments except that here the specimens were cathodically protected in order to form pure CaCO₃ scale on the steel surface while suppressing any Fe²⁺ release by corrosion and any formation of FeCO₃. During cathodic protection, the surface pH of the specimen was much higher than the bulk solution due to the artificial acceleration of hydrogen evolution reactions (HER) and consumption of hydrogen ions. Therefore, the surface water chemistry was favorable for precipitation of CaCO₃ scale in the absence of Fe²⁺. LPR and OCP measurements were performed once a day when the cathodic polarization was temporarily removed (for approximately 5 min) in order to observe the effect of CaCO₃ scale formation on corrosion rate and OCP. After 5 d, the cathodic protection was permanently halted, and one specimen was retrieved from the test solution for surface characterization while the other specimen (now covered with CaCO₃ scale)

[†]Trade name.

was exposed to the corrosive solution that was saturated with CaCO_3 .

EXPERIMENTAL RESULTS

4.1 | First Scenario: Mixed Iron-Calcium Carbonate

Within this research, a special effort was made to maintain very similar water chemistry for experiments based on the test matrix presented in Table 1. Figure 2 shows the bulk solution pH for experiments with and without Ca^{2+} over time. Solution pH was maintained at pH 5.5 by adding hydrochloric acid (HCl) when it was necessary during the experiment without the presence of Ca^{2+} . However, the CaCO_3 -saturated solution showed a strong buffering capacity over the course of experiments; therefore, the solution pH was self-controlled (autogenous) at its initial value of pH 5.5. Such buffering behavior in presence of CaCO_3 was also reported by Duan and Li.⁴⁰ The saturation degree of FeCO_3 (S_{FeCO_3}) is a crucial parameter in CO_2 corrosion that influences precipitation rate of FeCO_3 and thus the corrosion behavior.⁴¹ Figure 3 compares the FeCO_3 saturation degree of the bulk solution for experiments with and without Ca^{2+} over time. S_{FeCO_3} was calculated using Equation (1):

$$S_{\text{FeCO}_3} = \frac{C_{\text{Fe}^{2+}} \times C_{\text{CO}_3^{2-}}}{K_{\text{sp,FeCO}_3}} \quad (1)$$

where $C_{\text{Fe}^{2+}}$ and $C_{\text{CO}_3^{2-}}$ are ferrous ion (Fe^{2+}) and carbonate ion (CO_3^{2-}) concentrations in the bulk solution. The concentration of Fe^{2+} was measured while that of CO_3^{2-} was calculated based on the measured pH and using an equilibrium model for CO_2 speciation in aqueous environments.⁴² The $K_{\text{sp,FeCO}_3}$ in Equation (1) is the solubility product of FeCO_3 calculated using an equation proposed by Sun, et al.⁴³

$$\log K_{\text{sp,FeCO}_3} = -59.3498 - 0.041377 \times T_k - \frac{2.1963}{T_k} + 24.5724 \times \log(T_k) + 2.518 \times I^{0.5} - 0.657 \times I \quad (2)$$

In Equation (2), T_k is the temperature (in Kelvin) and I is the ionic strength. Fe^{2+} was introduced into the bulk solution by the corrosion process and, as a result, FeCO_3 saturation increased over time for all experiments irrespective of Ca^{2+} concentration. However, the final value of FeCO_3 saturation for the experiment without Ca^{2+} was higher than the experiment with Ca^{2+} due to its higher corrosion rate, leading to a higher Fe^{2+} concentration in the bulk. The final FeCO_3 saturation value for experiments with and without Ca^{2+} was 1.2 and 10.8, respectively (see Figure 3).

The LPR corrosion rate of the steel specimens for experiments conducted in the presence of 6,000 ppm Ca^{2+} (solution was saturated with respect to CaCO_3) is compared with that of baseline conditions (in the absence of Ca^{2+} ions) in Figure 4 using a B value of 26 mV/decade. This value is commonly accepted in CO_2 environments but is not based on any specific Tafel slopes as the corrosion mechanism is not strictly charge transfer controlled. Instead, this B value was determined by best fit comparison between current densities and WL measurements.⁴⁴⁻⁴⁵ The error bars in Figure 4 and other figures throughout this article represent the maximum and

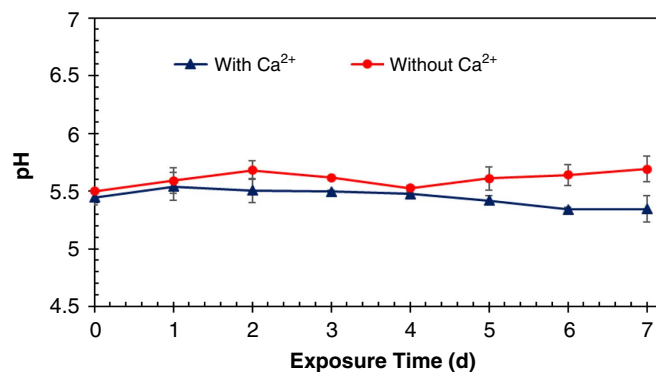


FIGURE 2. Variation of bulk solution pH over time for experiments with and without 6,000 ppm Ca^{2+} ($S_{\text{CaCO}_3} = 1$) at 80°C , $p\text{CO}_2$ 0.53 bar, 0.60 M ionic strength, and 20 rpm.

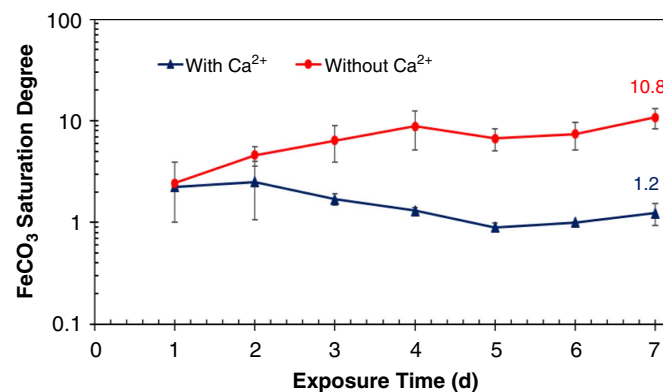
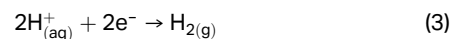


FIGURE 3. Variation of FeCO_3 saturation degree over time for the experiments with and without 6,000 ppm Ca^{2+} ($S_{\text{CaCO}_3} = 1$) at 80°C , $p\text{CO}_2$ 0.53 bar, bulk solution pH 5.5, 0.60 M ionic strength, and 20 rpm.

minimum values at each data point obtained in two repeated of the same experiment.

Three corrosion regions were identified in both experiments (see Figure 4): 1. active corrosion, 2. nucleation and growth of carbonates layer, and 3. pseudo-passivation. In this paper, "pseudo-passivation" refers to the decrease in corrosion rate observed with a simultaneous increase in corrosion potential.⁴⁴

The initial increase in the corrosion rate is related to the presence of a semiconductive cementite phase (Fe_3C) that is commonly reported as the early-stage corrosion product for ferritic-pearlitic steels, such as UNS G10180⁽¹⁾ steel.⁴⁶ Fe_3C is typically found on the surface of corroded steel and is due to the preferential dissolution of the ferrite phase ($\alpha\text{-Fe}$) over Fe_3C in the corrosion process. The presence of Fe_3C increases the steel corrosion rate through a galvanic effect as it provides more cathodic sites for the HER.⁴⁷⁻⁴⁸ The main HER in CO_2 aqueous environments is described as follows:



As can be seen from Figure 4, the active corrosion region was shorter and the LPR corrosion rate was lower in the presence of Ca^{2+} . However, for both experiments, corrosion rates decrease after reaching a maximum value of 9 mm/y and 19 mm/y for experiments with and without Ca^{2+} , respectively. It worth mentioning that the magnitude of corrosion rate obtained by LPR can be exaggerated. This is due to the inability of the LPR technique to cope with the galvanic corrosion effect inherited

⁽¹⁾ UNS numbers are listed in *Metals & Alloys in the Unified Numbering System*, published by the Society of Automotive Engineers (SAE International) and cosponsored by ASTM International.

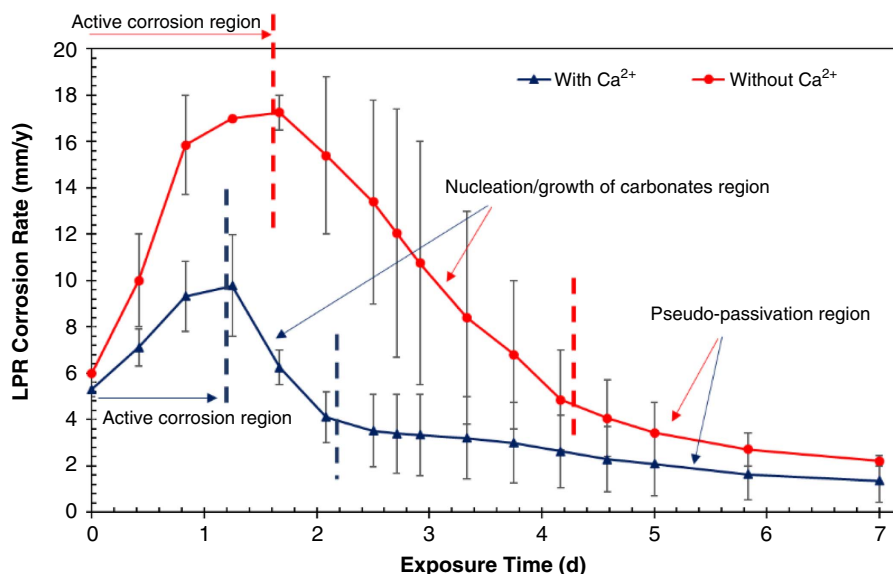


FIGURE 4. Comparison of LPR corrosion rates of UNS G10180 exposed to solutions without and with 6,000 ppm Ca^{2+} ($S_{\text{CaCO}_3} = 1$) at 80°C, $p\text{CO}_2$ 0.53 bar, bulk solution pH 5.5, 0.60 M ionic strength, and 20 rpm.

from the active corrosion region. However, LPR data are here used for trends rather than for obtaining values of corrosion rates which are measured more accurately by WL method.

Cross-sectional characterization and SEM/EDS analysis were performed on the specimens retrieved from the test solutions at the different exposure times for both series of experiments. Such investigations revealed that the decrease of corrosion rate was due to nucleation and growth of carbonate layers within the Fe_3C network and adjacent to the steel surface. (Results of surface characterization are discussed in more detail in the *Surface Layer Characterization* Section). In the pseudo-passivation region, the corrosion rates with and without Ca^{2+} were reduced significantly. This was attributed, in part, to the fact that corrosion product layers became denser and more compact during this time. It should be mentioned that the residual corrosion rate in this region remained high both for experiments with and without Ca^{2+} (see Figure 4). Other researchers have also observed the same results, as the corrosion product layer could not offer a good level of protectiveness at low bulk solution pH (i.e., pH 5.5).⁴⁹ However, the final corrosion rate was lower in the presence of Ca^{2+} . This could indicate that the corrosion products in the presence of Ca^{2+} were comparatively more protective. However, the final corrosion rate was very similar for both tests. Two specimens were retrieved from the test solutions at days 2, 4, and 7 of the experiments for surface layer characterizations and measuring corrosion rate by WL techniques. Figure 5 depicts a comparison of time-averaged, cumulative, corrosion rate by WL (bar chart) and LPR (line chart) at different exposure times. LPR shows a higher corrosion rate than WL at each measuring point regardless of the presence of Ca^{2+} . This graph also indicates that the corrosion rate without Ca^{2+} is higher than the experiments with Ca^{2+} at each measuring point, confirmed by both WL and LPR methods. Similarly to the corrosion obtained by LPR, WL methods showed that the corrosion rate was decreasing over time for both series of experiments.

A comparison of OCP in solutions with and without Ca^{2+} is shown in Figure 6. The initial OCP for both experiments was almost the same and it became more positive after the carbonate layers formed on the steel surface. Note that the OCP

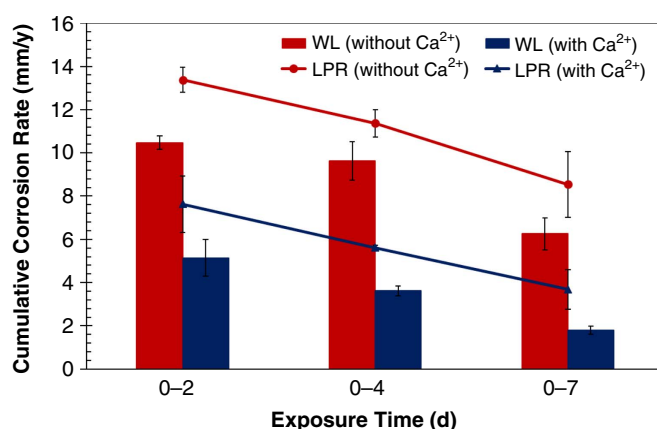


FIGURE 5. WL and LPR cumulative corrosion rate over time for solutions without and with 6,000 ppm Ca^{2+} ($S_{\text{CaCO}_3} = 1$) at 80°C, $p\text{CO}_2$ 0.53 bar, bulk solution pH 5.5, 0.60 M ionic strength, and 20 rpm.

values at the end of experiments with the presence of Ca^{2+} are greater, indicating a better protectiveness offered by the surface layers in pseudo-passivation region.

4.2 | Surface Layer Characterization

Surface layers were characterized using a JEOL JSM-6390LV[†] SEM. The chemical composition of the corrosion products and scales was analyzed by a Bruker[†] EDS detector attached to the SEM.

4.2.1 | Experiments Without Ca^{2+}

Figure 7 shows SEM cross-sectional and top view images of surface layers developed at different exposure times for experiments conducted in the absence of Ca^{2+} . The yellow arrows on the cross-sectioned specimens indicate the calculated metal loss based on WL corrosion rate. Such values were greater than the measured physical thickness of the Fe_3C layer, indicating that shear stress created by flow could have removed some of the Fe_3C from the steel surface, particularly in the beginning of the experiments.⁵⁰ Given that Fe_3C is a fragile

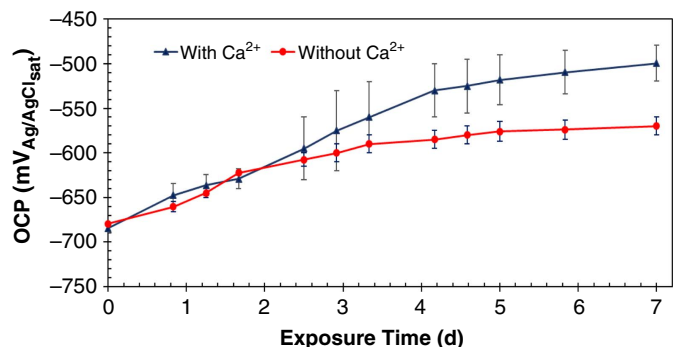


FIGURE 6. Comparison of OCP over time for UNS G10180 exposed to solutions without and with 6,000 ppm Ca²⁺ ($S_{CaCO_3} = 1$) at 80°C, pCO_2 0.53 bar, bulk solution pH 5.5, 0.60 M ionic strength, and 20 rpm.

corrosion product, its partial removal in the early stage of the corrosion process is possible. However, precipitation of FeCO₃ within the pores of Fe₃C, in the later stages of the corrosion process, would indirectly increase its mechanical strength.

Top and cross-sectional images taken for the first 2 d of the experiment confirm the development of a porous Fe₃C layer with an approximate thickness of 24 μm. Comparatively, Figure 4 indicates that the corrosion rate at the end of the second day (active corrosion region) was at a maximum value of 19 mm/y. The cross-section image at the end of day 4 suggests that a second phase precipitated within the Fe₃C network, adjacent to the steel surface. This second layer composition as determined by EDS analysis (see Figure 8) was consistent with FeCO₃.²⁷ Upon the precipitation of FeCO₃ within the Fe₃C pores, the corrosion rate decreased and so did the layer growth rate from day 4 to day 7. A scan of the top view images at different

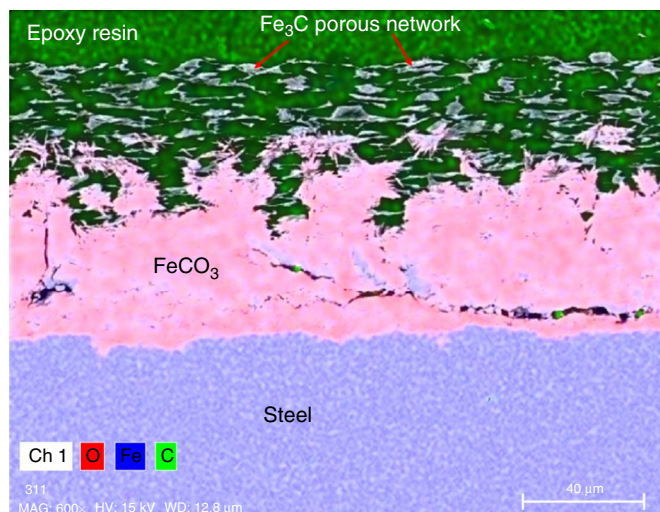


FIGURE 8. Cross-section SEM/EDS analysis of the corrosion products after 7-d exposure to the experiment without Ca²⁺ at 80°C, pCO_2 0.53 bar, bulk solution pH 5.5, 0.60 M ionic strength, and 20 rpm.

exposure times suggests that FeCO₃ crystals did not precipitate on top of the Fe₃C layer, even though FeCO₃ saturation degree for the bulk solution reached a value of 10.8 by the end of the experiment. In fact, the development of a Fe₃C network hindered the mass transfer of Fe²⁺ outward from the steel surface and resulted in a much higher concentration of Fe²⁺ near the steel surface compared to the bulk solution. Indeed, the occurrence of HERs within the Fe₃C network and on the steel surface increased the solution pH in these areas as well, leading to high supersaturation with respect to FeCO₃. Therefore, a different water chemistry compared to the bulk aqueous

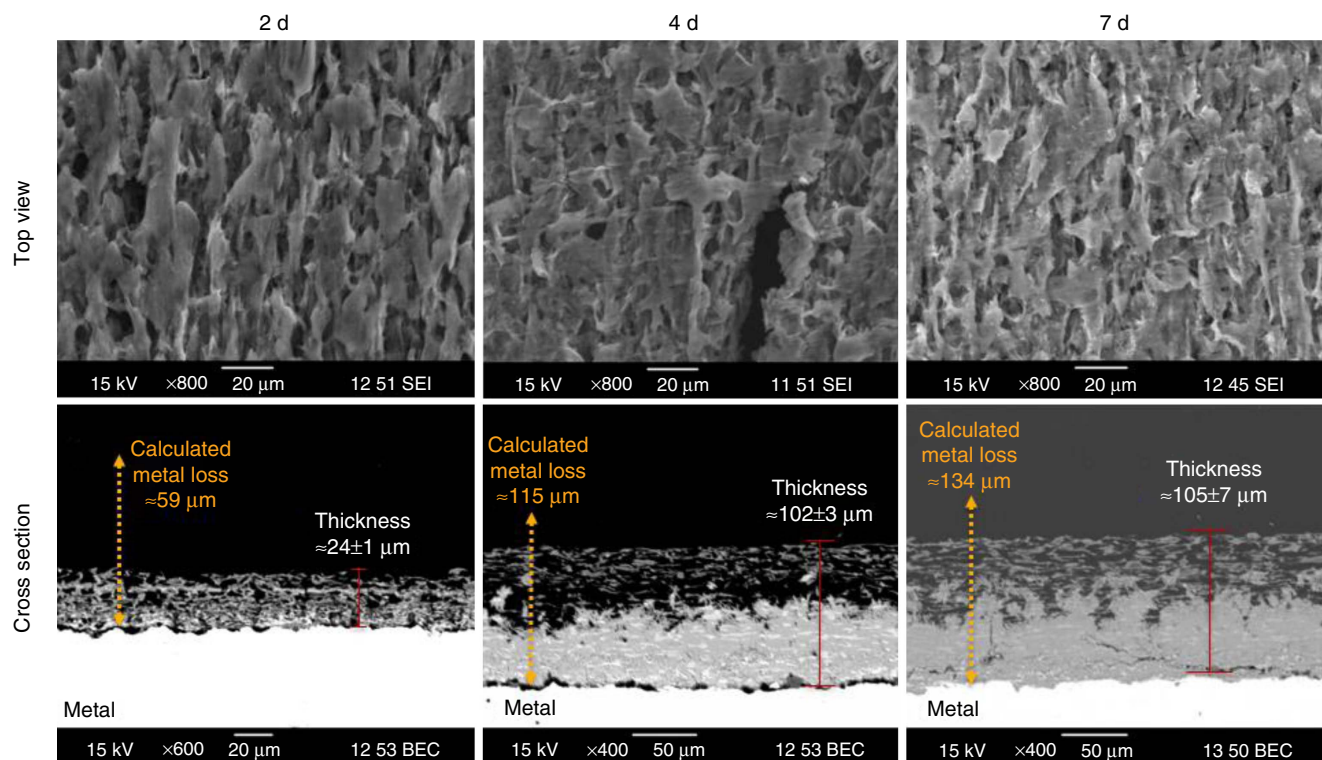


FIGURE 7. SEM images (top and cross-section view) of the development of surface layers over time for the experiment without Ca²⁺ at 80°C, pCO_2 0.53 bar, bulk solution pH 5.5, 0.60 M ionic strength, and 20 rpm.

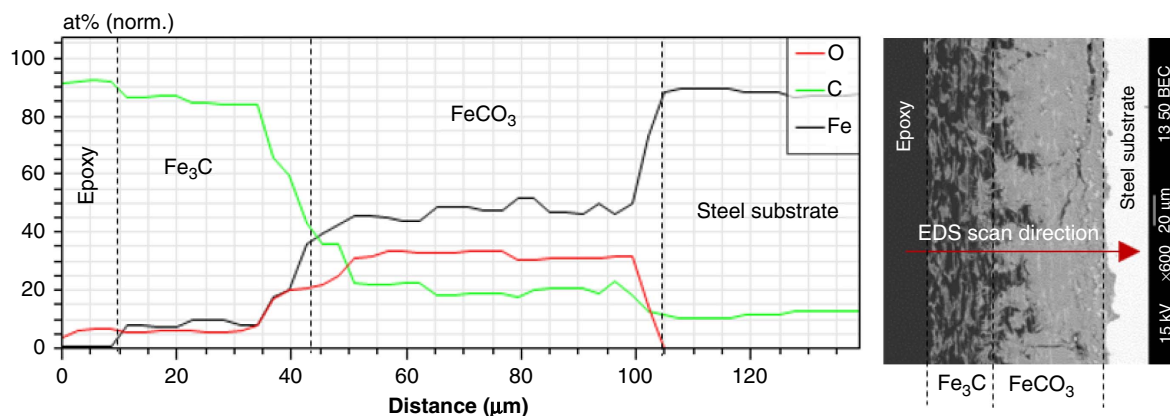


FIGURE 9. EDS line scan analysis of the surface layers developed after 7-d exposure to the experiment without Ca^{2+} at 80°C , $p\text{CO}_2$ 0.53 bar, bulk solution pH 5.5, 0.60 M ionic strength, and 20 rpm.

environment was achieved within the Fe_3C network, which favored precipitation of FeCO_3 adjacent to the steel surface,⁵¹ evident from the cross-section SEM images at the end of day 4 and day 7 of the experiment. To provide more proof of such a phenomenon, Figure 9 shows an elemental line scan of the surface layers developed after 7-d exposure that suggests precipitation of FeCO_3 adjacent to the steel surface.

The analysis provided here for the experiments conducted in the absence of Ca^{2+} constitutes a necessary baseline experiment used to identify the effect of the presence of Ca^{2+} on the experimental results. Indeed, a series of recent publications using in situ synchrotron XRD have provided great insight into the mechanism of corrosion product development in CO_2 corrosion of mild steel. These studies were performed in the absence of Ca^{2+} and for relatively short-term exposures.⁵²⁻⁵⁵ Such studies have also emphasized the importance of local supersaturation

and surface conditions. In addition, the authors Ko, et al., proposed that iron dissolution leads to the formation of colloidal FeCO_3 and to the growth of solid FeCO_3 through an electrocrystallization process.⁵⁵ Caution should be taken regarding generalizations of the authors' findings to the present work as the electrochemical measurements were conducted under significant perturbations from the equilibrium state (primarily due to the limited timeframe for synchrotron analysis) resulting in somehow artificial local water chemistries at the steel surface, which deviate significantly from the bulk aqueous environment.³⁸

4.2.2 | Experiments with Ca^{2+} (CaCO_3 Saturation Degree of Unity and 6,000 ppm Ca^{2+})

Figure 10 shows SEM images (cross-section and top view) of surface layers developed at different exposure times

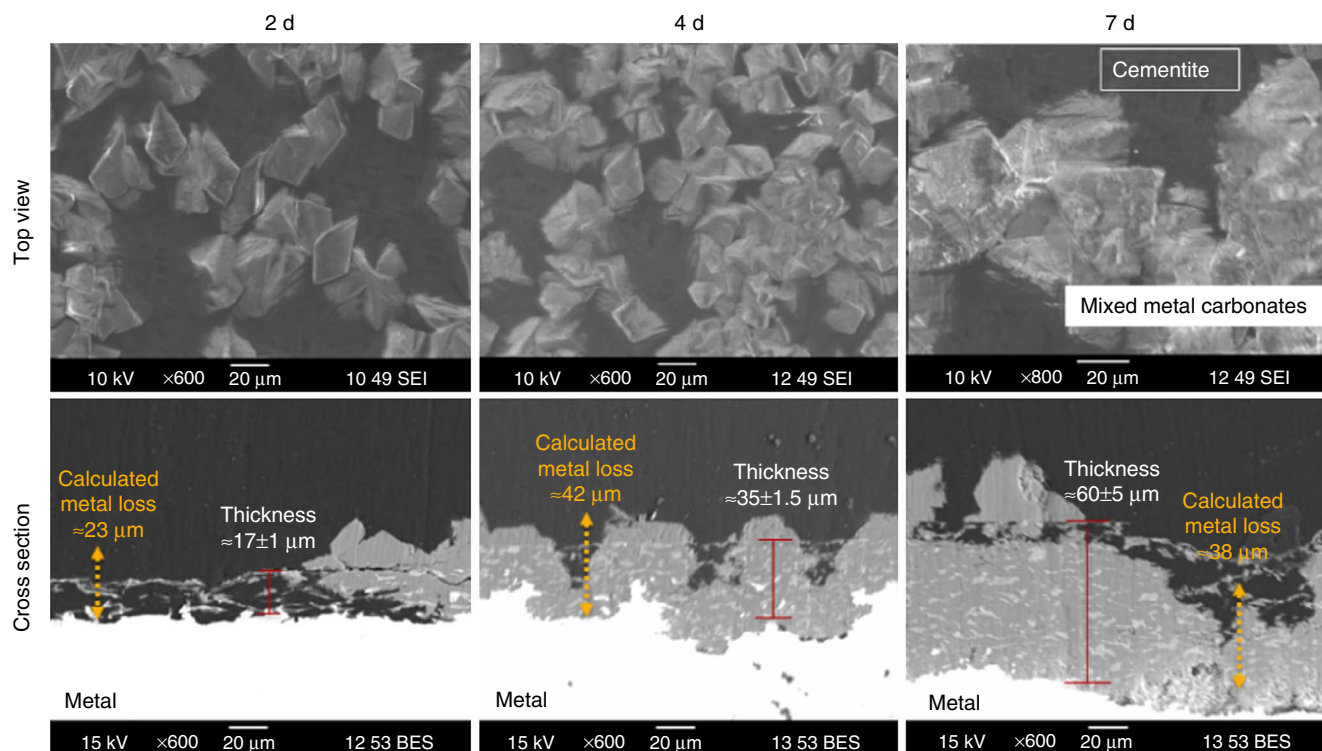


FIGURE 10. SEM images (top and cross-section view) of the development of surface layers over time for the experiments conducted in the presence of 6,000 ppm Ca^{2+} ($S_{\text{CaCO}_3} = 1$) at 80°C , $p\text{CO}_2$ 0.53 bar, bulk solution pH 5.5, 0.60 M ionic strength, and 20 rpm.

for an experiment with a CaCO_3 -saturated solution. Unlike the experiment conducted in the absence of Ca^{2+} , SEM images of the top view confirmed precipitation of crystalline phases on the top of the steel surface after 2 d of exposure only. Such crystals did not cover the entire surface and their quantity and size grew over time (see top view images in Figure 10). EDS analysis and XRD data confirmed, see Figure 13, that such crystalline phases were a substitutional iron-calcium carbonate solid solution, with calcium being dominant over iron ($\text{Fe}_x\text{Ca}_y\text{CO}_3$, $x + y = 1$ and $x < y$). The cross-sectional SEM image of the specimen after 2 d of exposure confirmed that $\text{Fe}_x\text{Ca}_y\text{CO}_3$ was partially precipitated within the Fe_3C porous structure. Fe_3C developed as the initial corrosion product on the steel surface. The thickness of the Fe_3C layers at this time was around $17 \mu\text{m}$. A much higher pH value would have occurred within the Fe_3C pores in comparison to the pH 5.5 of the bulk solution. The bulk solution was already saturated with respect to CaCO_3 at 80°C , pH 5.5, $p\text{CO}_2$ 0.53 bar, 0.60 M ionic strength, and $[\text{Ca}^{2+}] \approx 6,000$ ppm. The increased pH within the Fe_3C network would favor precipitation of CaCO_3 . However, due to its presence close to the steel surface, Fe^{2+} would also be involved in the crystallization process, along with Ca^{2+} and a substitutional solid solution of iron-calcium carbonate with Ca being dominant over Fe formed at this stage. Precipitation of mixed carbonates first started within the Fe_3C network; however, propagation and growth of such phases continued out of the Fe_3C layers, which in some locations were visible from top view and cross-section images as shown in Figure 10. Based on Figure 4, the corrosion rate was still increasing up to day 2 of the experiment without Ca^{2+} , whereas for the experiment with 6,000 ppm Ca^{2+} , the corrosion rate was already decreasing by day 2. This decrease was due to precipitation of the mixed metal carbonate within the Fe_3C and partial blockage of the steel surface, retarding the anodic reaction. Cross-section morphology of the surface layers at the end of day 4 showed that almost the entire Fe_3C layer was filled with $\text{Fe}_x\text{Ca}_y\text{CO}_3$. The corrosion rate obtained by LPR

showed a high value of 2.3 mm/y at this stage (Figure 4). An immediate conclusion was that precipitation of $\text{Fe}_x\text{Ca}_y\text{CO}_3$ on the steel surface could not offer an acceptable level of protection against further corrosion, and undermining corrosion was still ongoing. This explains why the thickness of surface layers grew from $35 \mu\text{m}$ at day 4 to $60 \mu\text{m}$ at day 7 of the experiment.

Figure 11 illustrates the chemical composition obtained by EDS of the surface layers after 7-d exposure to the solution saturated with CaCO_3 . For better visualization, the graph is divided into six zones, from (a) to (f), with different colors. Zone (a) corresponds to the epoxy resin, used for the preparation of specimens for cross-section, with carbon and oxygen being the constituent elements. The line scan enters the cementite structure in zone (b), with carbon and iron being the principal constituent elements. Zone (c) confirms the formation of a mixed solid solution of $\text{Fe}_x\text{Ca}_y\text{CO}_3$ where the mole fraction of Ca is greater than Fe ($y > x$). Therefore, this compound is named "scale" rather than "corrosion product" as Ca is dominant over Fe. This zone comprises the main portion of surface layers with an approximate thickness of $45 \mu\text{m}$. Zone (d) begins with at a point where the mole fractions of Ca and Fe are equal within the solid solution of $\text{Fe}_x\text{Ca}_y\text{CO}_3$ ($x = y$). However, closer to the steel surface, the mole fraction of Fe becomes dominant over Ca. Therefore, the surface layer precipitated in this zone is considered a "corrosion product" with the partial incorporation of Ca. Zone (e) is located very close to the steel surface. In this zone, Ca is not present and a pure FeCO_3 is formed. Eventually, the line scan enters the steel substrate in zone (f). The presence of carbon in this zone is mainly considered to be a contamination from epoxy resin during conservation of the corrosion product layer and the polishing process.

Figure 12 (EDS mapping) clearly illustrates the formation of $\text{Fe}_x\text{Ca}_y\text{CO}_3$ within and outside the Fe_3C network, along with the formation of FeCO_3 adjacent to the steel surface. As mentioned earlier, the change of water chemistry near the steel

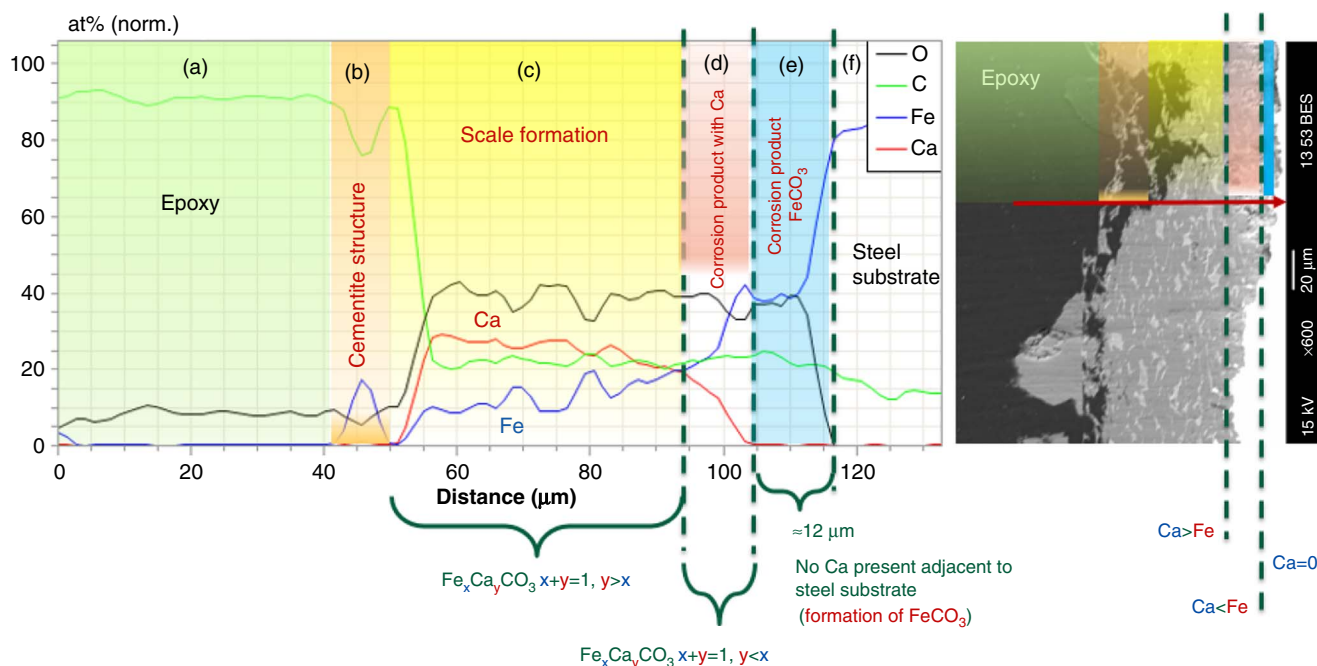


FIGURE 11. EDS analysis (line scan) of the surface layers formed on carbon steel after 7-d exposure to a solution with the presence of 6,000 ppm Ca^{2+} ($S_{\text{CaCO}_3} = 1$) at 80°C , $p\text{CO}_2$ 0.53 bar, bulk solution pH 5.5, 0.60 M ionic strength, and 20 rpm.

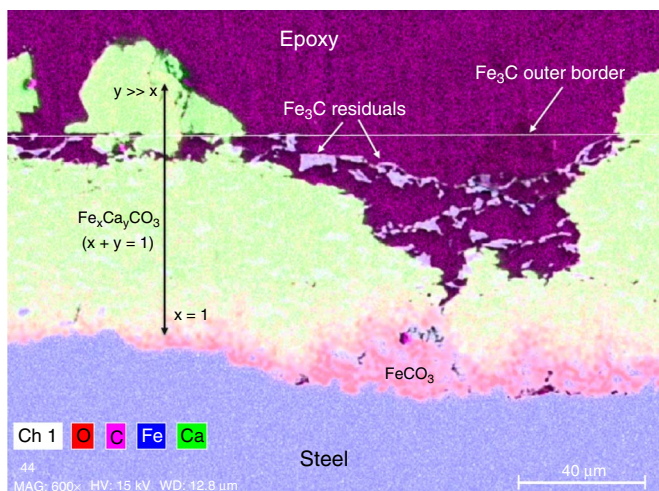


FIGURE 12. EDS analysis (map mode) of a cross-section UNS G10180 specimen after 7-d exposure to a CaCO_3 -saturated solution at 80°C , bulk solution pH 5.5, $p\text{CO}_2$ 0.53 bar, 0.60 M ionic strength, and 6,000 ppm Ca^{2+} .

surface and within the Fe_3C pores was the main driving force for precipitation of the mixed carbonates. Figure 13 shows the XRD patterns of the surface layers after 7-d exposure to the solution saturated with respect to CaCO_3 . Although x-ray penetration power is limited and cannot reach the layers close to the steel surface, it is able to provide information relevant to the outer side of the surface layers. As can be seen in Figure 13, the detected carbonate peaks in the presence of Ca^{2+} ions are broadened and located between the reference peaks for CaCO_3 and FeCO_3 . This indicates the formation of a heterogeneous solid solution with a chemical formula of $\text{Fe}_x\text{Ca}_y\text{CO}_3$. Peaks associated with $\alpha\text{-Fe}$ and Fe_3C are also present in the detected XRD data. This could mean that the $\text{Fe}_x\text{Ca}_y\text{CO}_3$ phase did not cover the entire steel surface.

The vulnerability of the specimens to localized corrosion was also evaluated. Profilometry of the specimen surfaces was performed after removing corrosion product layers by Clarke's solution, according to ASTM Standard G1,⁵⁶ and no localized corrosion was observed for experiments with or without Ca^{2+} at the conducted experimental condition. For instance, Figure 14 illustrates the results of surface profilometry of a specimen

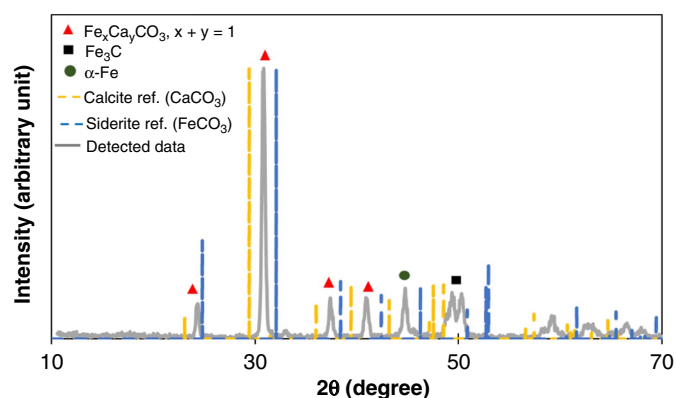


FIGURE 13. XRD pattern of the surface layers formed on UNS G10180 specimen after 7-d exposure to a CaCO_3 -saturated solution (6,000 ppm Ca^{2+}) at 80°C , bulk solution pH 5.5, $p\text{CO}_2$ 0.53 bar, 0.60 M ionic strength, and 20 rpm.

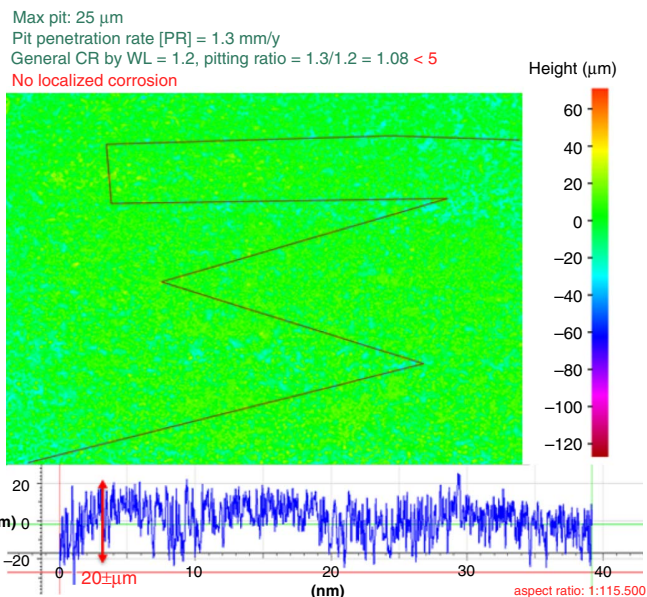


FIGURE 14. Surface profilometry of the specimen exposed to CaCO_3 -saturated solution after 7 d revealed no localized corrosion.

exposed to a CaCO_3 -saturated solution after 7 d. The maximum penetration rate is 1.3 mm/y, based on a maximum measured pit of 25 μm . The WL corrosion rate for this specimen is 1.2 mm/y, which yields a pitting ratio of ≈ 1 (pitting ratio = penetration rate/WL corrosion rate). A pitting ratio of 5 or above has been commonly proposed as a requirement to qualify localized corrosion.⁵⁷ None of the specimens exposed to corrosion environments in this study had a pitting ratio higher than 5.

4.3 | A Descriptive Model (First Scenario: Mixed Iron-Calcium Carbonate)

Based on the experimental results, a descriptive model is proposed for the mechanism of CO_2 corrosion of mild steel (with ferritic-pearlitic microstructure) exposed to a CaCO_3 -saturated solution with a high concentration of Ca^{2+} at 80°C , bulk solution pH 5.5, $p\text{CO}_2$ 0.53 bar, 0.60 M ionic strength:

- UNS G1018 carbon steel is exposed to solution saturated with CaCO_3 and CO_2 as shown in Figure 15(a);
- Fe dissolves and Fe^{2+} is released into solution. Consequently, a porous Fe_3C network is left behind on the steel surface and grows in thickness over time, as shown in Figure 15(b);
- The Fe_3C layer reaches a critical thickness with a water chemistry very different within its pores ($S_{\text{CaCO}_3} \gg 1$) as compared to the bulk solution ($S_{\text{CaCO}_3} = 1$). This condition favors nucleation and growth of CaCO_3 . However, due to the presence of Fe^{2+} and isostructurality of calcite (CaCO_3) and siderite (FeCO_3), a substitutional carbonate, $\text{Fe}_x\text{Ca}_y\text{CO}_3$ ($x + y = 1$), forms within the pores of the Fe_3C network, as shown in Figure 15(c);
- At this stage, almost the entire Fe_3C network is filled with $\text{Fe}_x\text{Ca}_y\text{CO}_3$ ($x + y = 1$) with $y \gg x$ for the exterior of the surface layer, as shown in Figure 15(d);
- Although the corrosion rate decreases upon precipitation and development of $\text{Fe}_x\text{Ca}_y\text{CO}_3$ on the steel surface, undermining corrosion is ongoing and, as a result, the thickness of the surface layer grows over time, as shown in Figure 15(e);

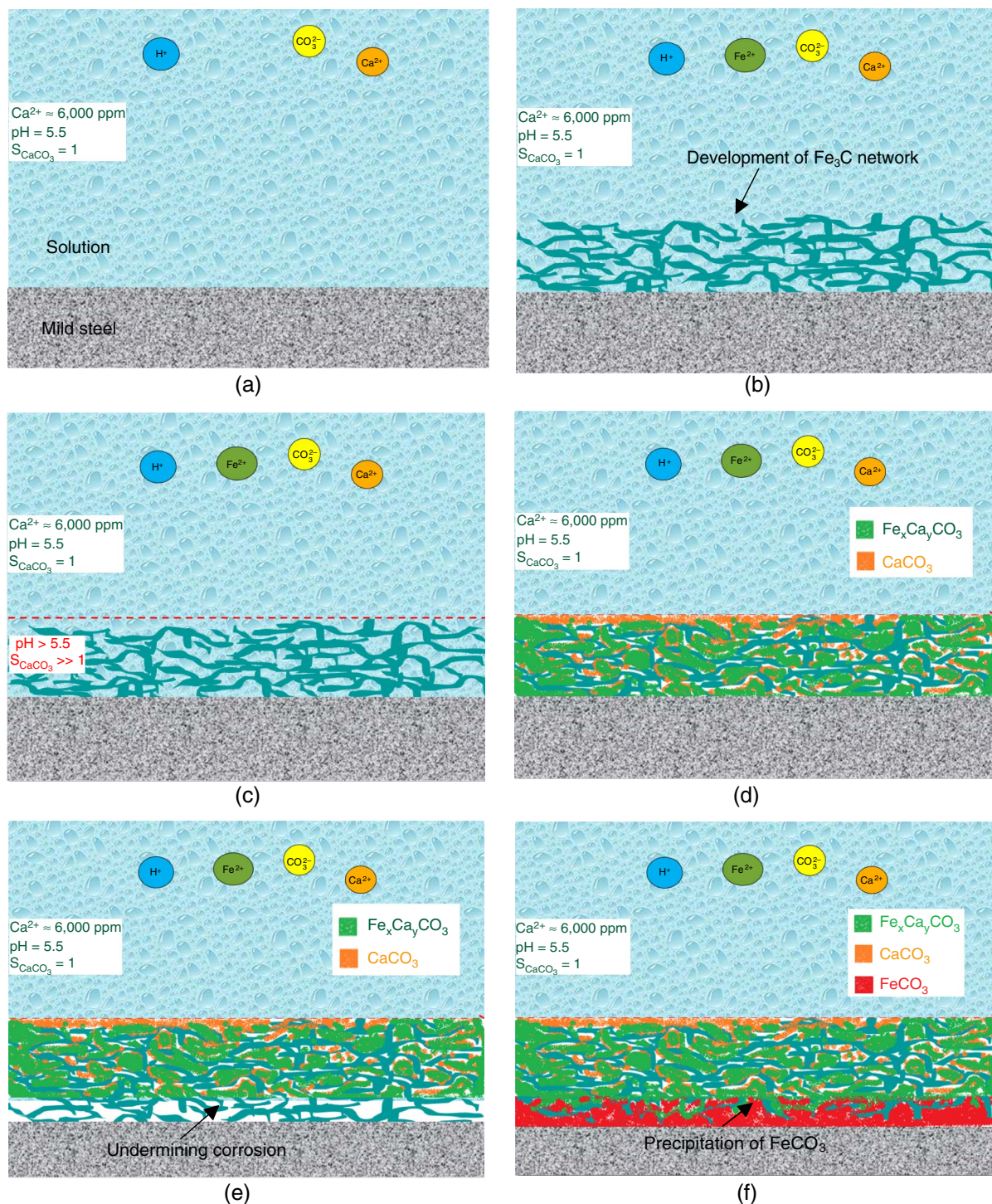


FIGURE 15. A descriptive model for CO₂ corrosion mechanism of mild steel exposed to the CaCO₃-saturated solution at 80°C, bulk solution pH 5.5, pCO₂ 0.53 bar, 6,000 ppm Ca²⁺, 0.60 M ionic strength, and 20 rpm.

(f) The presence of mixed carbonates on the steel surface hinders mass transfer of Fe²⁺ outward from the steel; therefore, the solubility limit of FeCO₃ is exceeded adjacent to the steel substrate and conditions and forms on the steel surface as an inner layer, as shown in Figure 15(f). Precipitation of FeCO₃ and its growth at this stage is responsible for the further decrease in corrosion rate.

4.4 | Second Scenario: Pure Calcium Carbonate

This section presents the results obtained in the second test series, focusing on determining the protectiveness of pure CaCO₃ when it forms uniformly. There are minimal data in the literature about the protectiveness of CaCO₃ scale (without incorporation of Fe) when it comes to CO₂ corrosion of mild steel, as all of the studies are related to situations when FeCO₃

and/or a mixed $\text{Fe}_x\text{Ca}_y\text{CO}_3$ form. The tests were performed using the same setup as for the previous section and following the conditions highlighted in Table 2. The analysis of the results presented below first focuses on the characteristics of the precipitated CaCO_3 scale and then address its protectiveness against CO_2 corrosion.

4.5 | Formation of Artificial CaCO_3 Scale

Figure 16 shows the morphology of the surface layer formed on the mild steel surface during 5-d exposure to the electrolyte and under continuous cathodic polarization. The SEM cross-section image reveals a uniform, thin and compact ($5\ \mu\text{m}$ to $7\ \mu\text{m}$) layer. The vertical cracks seen in the cross-section image are likely generated during the polishing process. The chemical composition analysis by EDS confirmed that this

surface layer is indeed pure CaCO_3 without any detectable incorporation of Fe. Figures 17 and 18 show EDS mapping and line scan analysis of the top and cross-section surface layers, respectively. Fe did not incorporate into CaCO_3 during its crystallization and pure CaCO_3 scale precipitated on the steel surface.

During the cathodic polarization of the specimens, the corrosion rate was measured once a day at its OCP. To achieve this, the cathodic polarization was temporarily interrupted for about 5 min, allowing the potential to reach its OCP and then LPR corrosion rate was measured. Figures 19(a) and (b) depict corrosion rate and potential trends (average OCP and cathodic potential) during the entire duration (5 d) of the experiment, respectively. The corrosion rate decreased over time upon precipitation of CaCO_3 scale on the steel surface. From the corrosion rate trend, it could be concluded that CaCO_3 scale can

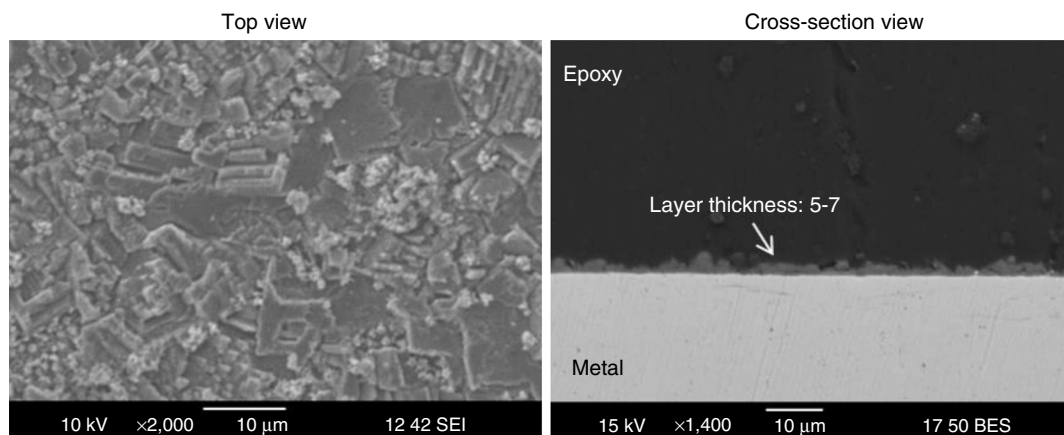


FIGURE 16. Top and cross-section view SEM of the surface layers formed on the steel during 5-d cathodic polarization; CaCO_3 -saturated solution (6,000 ppm Ca^{2+}), 80°C , bulk solution pH 5.5, $p\text{CO}_2$ 0.53 bar, 0.60 M ionic strength, and 20 rpm.

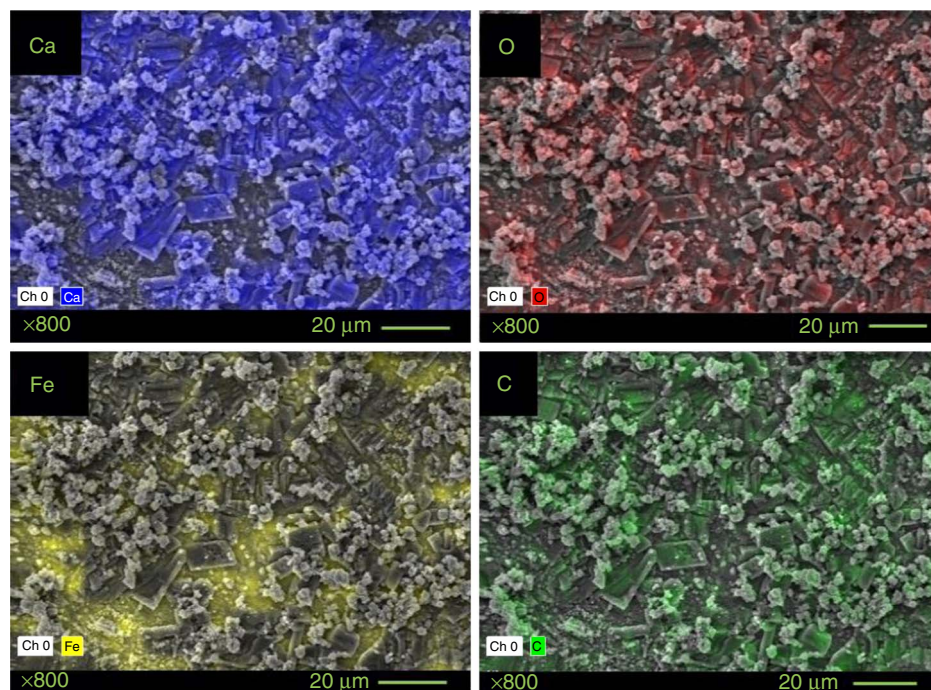


FIGURE 17. SEM and EDS mapping analysis of the surface layers formed during 5-d cathodic polarization; Fe is absent in the precipitated crystalline phases (80°C , bulk solution pH 5.5, $p\text{CO}_2$ 0.53 bar, 6,000 ppm Ca^{2+} , 0.60 M ionic strength, and 20 rpm).

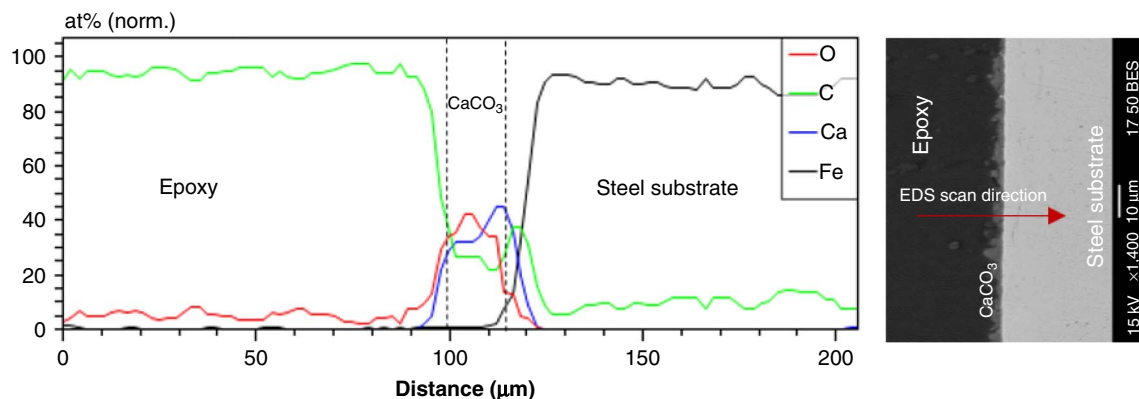


FIGURE 18. EDS line scan results showing distribution of Ca, C, O, and Fe within the surface layers; formation of CaCO_3 scale (80°C , bulk solution pH 5.5, $p\text{CO}_2$ 0.53 bar, 6,000 ppm Ca^{2+} , 0.60 M ionic strength, and 20 rpm).

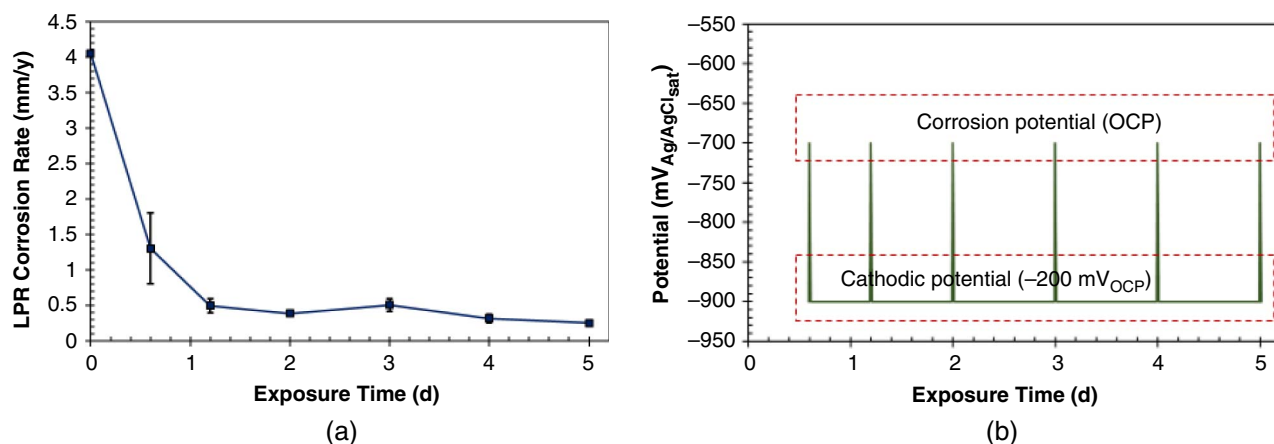


FIGURE 19. (a) LPR corrosion rate and (b) potential variations over time during cathodic polarization of the specimens (80°C , bulk solution pH 5.5, $p\text{CO}_2$ 0.53 bar, 6,000 ppm Ca^{2+} , 0.60 M ionic strength, and 20 rpm).

offer some protection against further corrosion. However, this is a premature conclusion because the metal was also cathodically protected in this period (even if it was interrupted periodically). The average OCP over time remained almost unchanged and it seemed that formation of CaCO_3 scale did not influence the OCP. One explanation for this observation is that CaCO_3 scale retarded the anodic and cathodic reactions at the same rate by decreasing the active surface area of the steel. A question remained whether or not this protectiveness could be retained after removing the cathodic polarization. This issue is addressed in the next section.

4.6 | Removing Cathodic Polarization

The CaCO_3 -covered specimen continued to be exposed to the corrosive solution (Table 2), but this time without cathodic polarization to investigate the protectiveness of the precipitated scale. Figures 20(a) and (b) show pH and Fe^{2+} variation over time, respectively, with and without cathodic polarization. The bulk solution was always saturated with respect to CaCO_3 , showing a strong buffering capability toward pH change at the conducted experimental conditions (Figure 20[a]). As can be seen from Figure 20(b), the corrosion rate was well controlled during the polarization period with no measurable Fe^{2+} in the bulk solution. Upon removal of the cathodic potential after day 5, Fe^{2+} concentration in the bulk solution increased over the

remaining 7 d of the experiment, indicating active corrosion of the steel surface. Figures 21(a) and (b) compare the corrosion rate obtained with LPR and potential between periods with and without cathodic protection. As can be seen in Figure 21(a), in the first 5 d (during cathodic protection), the corrosion rate decreased over time with the formation of CaCO_3 scale. However, after removing the cathodic protection, the corrosion seemed to first increase rapidly, reaching a similar level as that observed at the start of the experiment, and then was observed to decrease over the rest of the experimental duration. The corrosion behavior of the second period was more or less similar to the bare steel specimen exposed to the CaCO_3 -saturated solution (first experimental scenario described above). Figure 21(b) shows that the OCP was increasing over time after removal of cathodic protection. Such behavior is related to the surface layer development after exposure to the corrosion medium (without cathodic protection).

Figure 22 compares the SEM cross-sectional morphology of the specimens obtained with (a) and after removal (b) of the cathodic polarization. The surface layer thickness increased from 5 μm to 7 μm at the end of the polarization period to 17 μm to 25 μm after 7-d exposure to the CaCO_3 -saturated solution without cathodic polarization. The chemical composition analysis of the layers revealed that the CaCO_3 scale formed during polarization was still present as the outer layer and that a mixed

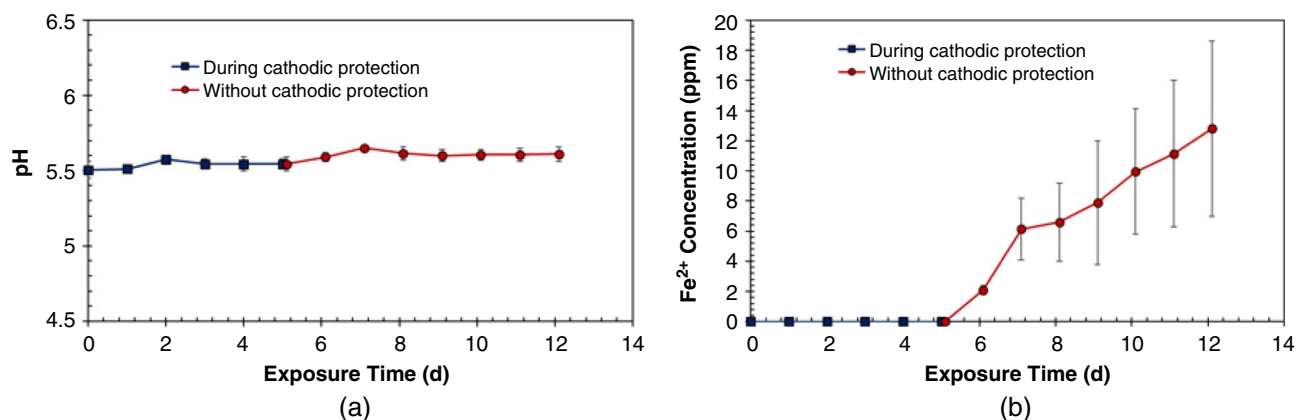


FIGURE 20. (a) pH and (b) Fe²⁺ concentration variation over time during and without cathodic protection (80°C, bulk solution pH 5.5, pCO₂ 0.53 bar, 6,000 ppm Ca²⁺, 0.60 M ionic strength, and 20 rpm).

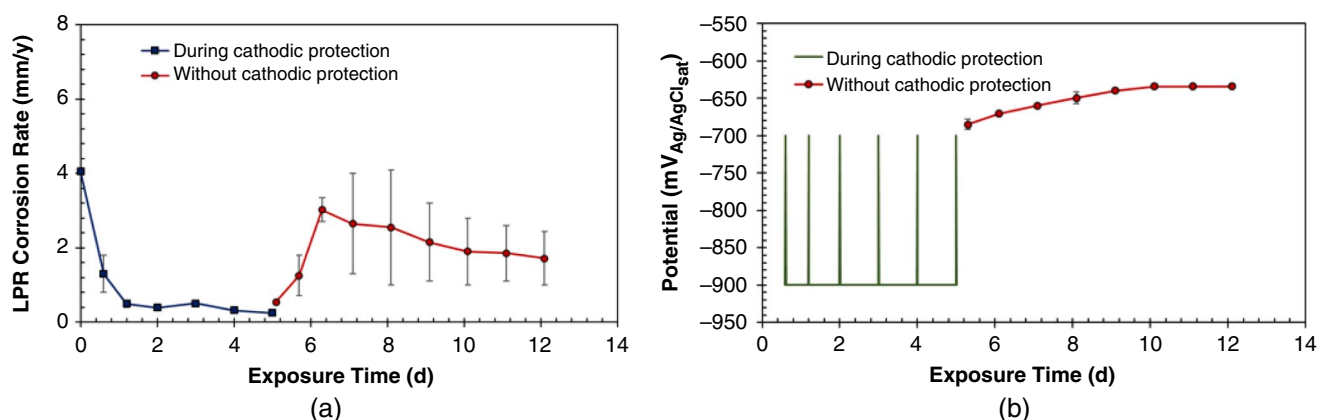


FIGURE 21. (a) Corrosion rate and (b) potential variation over time during and without cathodic protection (80°C, bulk solution pH 5.5, pCO₂ 0.53 bar, 6,000 ppm Ca²⁺, 0.60 M ionic strength, and 20 rpm).

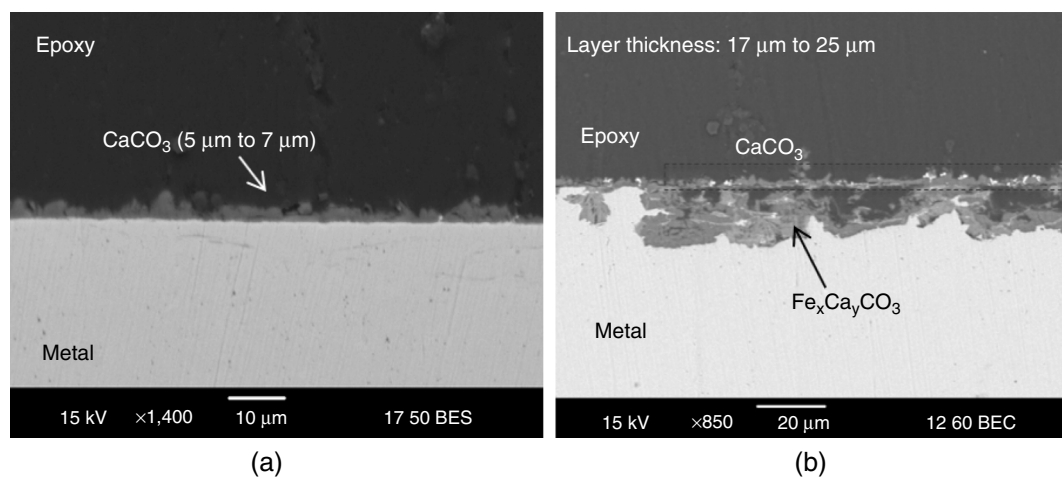


FIGURE 22. Comparison of surface layers morphology and thickness at the end of the polarization period (5-d exposure) and after exposure to the corrosive medium without cathodic protection (7-d exposure) at 80°C, bulk solution pH 5.5, pCO₂ 0.53 bar, 6,000 ppm Ca²⁺, 0.60 M ionic strength, and 20 rpm.

metal carbonate of Fe_xCa_yCO₃ was formed beneath the CaCO₃ layer, driven by corrosion processes as shown in Figure 23. Such analysis confirmed that although the corrosion rate decreased upon formation of CaCO₃ scale during polarization

(by reducing the anodic and cathodic reactions at the same rate), CaCO₃ scale did not maintain its protective behavior when exposed to the corrosive medium without cathodic polarization (active corrosion was observed). Such behavior of CaCO₃ scale is

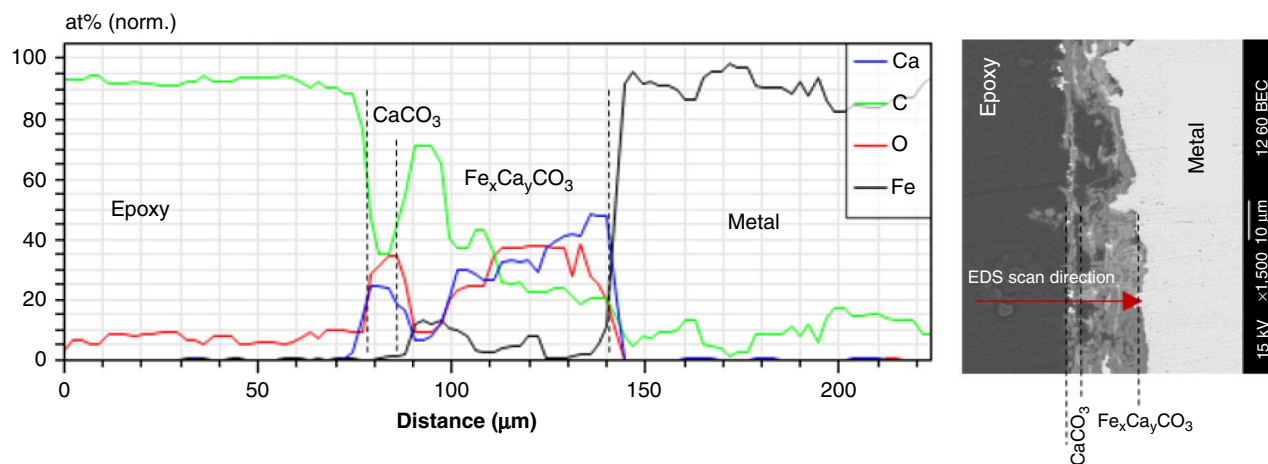


FIGURE 23. Chemical composition of the layers at the steel surface after 7-d exposure to a CaCO_3 -saturated solution without cathodic protection of specimen at pH 5.5, 80°C , 0.53 bar $p\text{CO}_2$, ionic strength 0.6 M, 6,000 ppm Ca^{2+} , and 20 rpm.

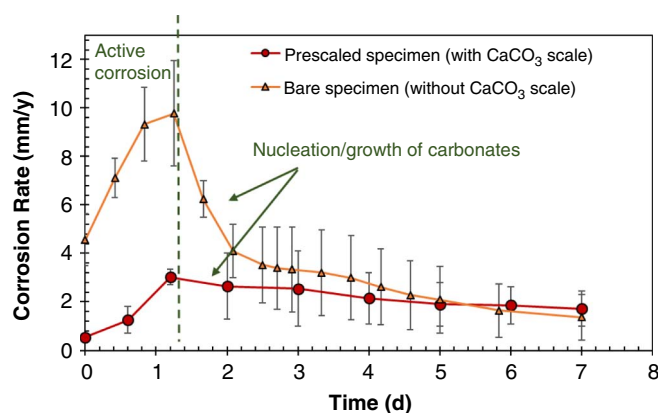


FIGURE 24. Comparison of corrosion behavior of mild steel with and without CaCO_3 scale at bulk solution pH 5.5, 80°C , 0.53 bar $p\text{CO}_2$, ionic strength 0.6 M, 6,000 ppm Ca^{2+} ($S_{\text{CaCO}_3} = 1$), and 20 rpm.

also reported by Ghanbari and Lillard in AC corrosion²⁹ and by Bekhrad and Javidi in the absence of dissolved Ca^{2+} ions.²⁸ It is noteworthy that despite CaCO_3 (scale) sharing a similar crystal structure to FeCO_3 (corrosion product), CaCO_3 did not show sustained protective behavior against further corrosion, while FeCO_3 is considered as a protective layer. The main argument is that the constituent cations of CaCO_3 scale and FeCO_3 have different sources. Ca^{2+} ions come from bulk solution, while Fe^{2+} ions come from the corroding steel surface. Therefore, FeCO_3 has superior adherence to steel with probably different mechanical properties. This is what makes FeCO_3 a more protective layer in comparison with CaCO_3 .

SUMMARY OF CORROSION MECHANISMS

Figure 24 compiles the results already presented for the two experiments described above and compares the corrosion rate trend over time of carbon steel considering two different starting conditions: a bare specimen and a specimen prescaled with CaCO_3 . The two specimens were exposed to the same experimental conditions described in Table 1, and no cathodic polarization was applied at that point. The purpose of this comparison is to investigate if the presence of CaCO_3 has any effect on the corrosion trend and on the steady-state

corrosion rate. The bare specimen showed a higher initial corrosion rate over the first days of the experiment compared to the prescaled specimens. However, the final corrosion rate of both specimens was identical at the end of the experiments. It can be concluded that CaCO_3 scale is not protective in the conducted experimental conditions. However, its presence accelerated the formation of $\text{Fe}_x\text{Ca}_y\text{CO}_3$ and/or FeCO_3 by hindering the mass transfer of Fe^{2+} from the steel surface to the bulk solution. For the bare specimen, the development of Fe_3C was also a mass transfer barrier for Fe^{2+} ; however, the galvanic effect between Fe_3C and $\alpha\text{-Fe}$ phases led to a pronounced acceleration of the corrosion rate, as compared to the prescaled specimens in the active corrosion zone.

CONCLUSIONS

The protectiveness of pure CaCO_3 and mixed $\text{Fe}_x\text{Ca}_y\text{CO}_3$ scale ($x + y = 1$ and $y > x$) was investigated in CaCO_3 -saturated solutions in the presence of high concentrations of Ca^{2+} . At the conducted experimental conditions ($S_{\text{CaCO}_3} = 1$, 80°C , bulk solution pH 5.5, $p\text{CO}_2$ 0.53 bar, 0.60 M ionic strength, and 6,000 ppm Ca^{2+}), the following conclusions can be made:

- CaCO_3 and $\text{Fe}_x\text{Ca}_y\text{CO}_3$ scale ($x + y = 1$ and $y > x$) acted as a mass transfer barrier and promoted surface conditions favoring FeCO_3 precipitation. The final decrease of corrosion rate was attributed to formation of FeCO_3 adjacent to the steel surface.
- CaCO_3 scale by itself was not protective against corrosion. Although CaCO_3 is isomorphous with FeCO_3 , Ca^{2+} ions come from bulk solution, while Fe^{2+} ions come from the corroding steel surface. The growth of FeCO_3 occurs immediately on the steel surface where Fe^{2+} is released. Therefore, FeCO_3 has superior adherence to the steel and offers protection against corrosion while CaCO_3 does not.
- Precipitation of CaCO_3 and $\text{Fe}_x\text{Ca}_y\text{CO}_3$ scale ($x + y = 1$ and $y > x$) did not seem to promote localized corrosion.

ACKNOWLEDGMENTS

The author also would like to thank the following companies for their financial support: Anadarko, Baker Hughes, BP, Chevron, CNOOC, ConocoPhillips, DNV GL, ExxonMobil, M-I SWACO (Schlumberger), Multi-Chem (Halliburton), Occidental Oil Company, PTT, Saudi Aramco, SINOPEC (China Petroleum), and TOTAL.

References

- C. de Waard, U. Lotz, D.E. Milliams, *Corrosion* 47, 12 (1991): p. 976-985.
- A. Kahyarian, B. Brown, S. Nešić, *Corrosion* 74, 8 (2018): p. 851-859.
- W. Li, B. Brown, D. Young, S. Nešić, *Corrosion* 70, 3 (2014): p. 294-302.
- K. Denpo, H. Ogawa, *Corrosion* 49, 6 (1993): p. 442-449.
- D. Ekawati, T. Berntsen, M. Seiersten, T. Hemmingsen, *Corrosion* 73, 9 (2017): p. 1157-1167.
- S. Nešić, L. Lunde, *Corrosion* 50, 9 (1994): p. 717-727.
- Y. Sun, T. Hong, C. Bosch, *Corrosion* 59, 8 (2003): p. 733-740.
- Z.D. Cui, S.L. Wu, S.L. Zhu, X.J. Yang, *Appl. Surf. Sci.* 252, 6 (2006): p. 2368-2374.
- K. Gao, F. Yu, X. Pang, G. Zhang, *Corros. Sci.* 50, 10 (2008): p. 2796-2803.
- J. Han, J.W. Carey, J. Zhang, *J. Appl. Electrochem.* 41, 6 (2011): p. 741-749.
- M. Kermani, A. Morshed, *Corrosion* 59, 8 (2003): p. 659-683.
- P.E. Dresel, A.W. Rose, "Chemistry and Origin of Oil and Gas Well Brines in Western Pennsylvania," The Pennsylvania State University, Open-File Report OFOG 10-01.0, 2010.
- H. Mansoori, R. Mirzaee, F. Esmaeilzadeh, A. Vojood, A. Soltan Dowrani, *Eng. Fail. Anal.* 82 (2017): p. 16-25.
- A. Rashedi, "A Study of Surface Wetting in Oil-Water Flow in Inclined Pipeline" (Master's thesis, Ohio University, 2016).
- H. Mansoori, R. Mirzaee, "On the Predictability of CO₂ Pitting Corrosion in Multiphase Gas Pipelines-An Upstream Case Study," CORROSION 2018, paper no. 10601 (Houston, TX: NACE International, 2018).
- H. Mansoori, D. Young, B. Brown, M. Singer, *J. Nat. Gas Sci. Eng.* 59 (2018): p. 287-296.
- A. Shamsa, R. Barker, Y. Hua, E. Barmatov, T.L. Hughes, A. Neville, *Corros. Sci.* 156 (2019): p. 58-70.
- S.N. Esmaeely, Y.-S. Choi, D. Young, S. Nešić, *Corrosion* 69, 9 (2013): p. 912-920.
- Y. Hua, A. Shamsa, R. Barker, A. Neville, *Appl. Surf. Sci.* 455 (2018): p. 667-682.
- S.N. Esmaeely, D. Young, B. Brown, S. Nešić, *Corrosion* 73, 3 (2017): p. 238-246.
- B. Wang, L. Xu, G. Liu, M. Lu, *Corros. Sci.* 136 (2018): p. 210-220.
- Z. Jia, C. Du, Z. Liu, J. Gao, X. Li, *Acta Metall. Sin.* 24, 5 (2011): p. 373-380.
- X. Jiang, Y.G. Zheng, D.R. Qu, W. Ke, *Corros. Sci.* 48, 10 (2006): p. 3091-3108.
- G.X. Zhao, L. Jian-Ping, H. Shi-Ming, L.U. Xiang-Hong, *J. Iron Steel Res. Int.* 12, 1 (2005): p. 38-42.
- C. Ding, K. Gao, C. Chen, *Int. J. Miner. Metall. Mater.* 16, 6 (2009): p. 661-666.
- L.M. Tavares, E.M. da Costa, J.J. de Oliveira Andrade, R. Hubler, B. Huet, *Appl. Surf. Sci.* 359 (2015): p. 143-152.
- H. Mansoori, D. Young, B. Brown, S. Nešić, M. Singer, *Corros. Sci.* 158 (2019): article id 108078.
- S. Bekhrad, M. Javidi, *J. Mater. Eng. Perform.* 28 (2019): p. 1057-1066.
- E. Ghanbari, R.S. Lillard, *Corrosion* 74, 5 (2018): p. 551-565.
- E.T. Urbansky, *Bioremediation J.* 2, 2 (1998): p. 81-95.
- H.Y. Ma, C. Yang, G.Y. Li, W.J. Guo, S.H. Chen, J.L. Luo, *Corrosion* 59, 12 (2003): p. 1112-1119.
- Z. Xia, K.-C. Chou, Z. Szklarska-Smialowska, *Corrosion* 45, 8 (1989): p. 636-642.
- M. Ergun, A.Y. Turan, *Corros. Sci.* 32, 10 (1991): p. 1137-1142.
- N.G. Smart, J.O. Bockris, *Corrosion* 48, 4 (1992): p. 277-280.
- E. McCafferty, N. Hackerman, *J. Electrochem. Soc.* 119, 8 (1972): p. 999-1009.
- N.A. Darwish, F. Hilbert, W.J. Lorenz, H. Rosswag, *Electrochim. Acta* 18, 6 (1973): p. 421-425.
- W.B. Fortune, M.G. Mellon, *Ind. Eng. Chem. Anal. Ed.* 10, 2 (1938): p. 60-64.
- R. Barker, D. Burkle, T. Charpentier, H. Thompson, A. Neville, *Corros. Sci.* 142 (2018): p. 312-341.
- A. Kahyarian, M. Achour, S. Nešić, "CO₂ Corrosion of Mild Steel," in *Trends in Oil and Gas Corrosion Research and Technologies* (Amsterdam, The Netherlands: Elsevier, 2017).
- Z. Duan, D. Li, *Geochim. Cosmochim. Acta* 72, 20 (2008): p. 5128-5145.
- S. Nešić, *Corros. Sci.* 49, 12 (2007): p. 4308-4338.
- S. Nešić, "Carbon Dioxide Corrosion of Mild Steel," in *Uhlig's Corrosion Handbook*, vol. 51 (Hoboken, NJ: John Wiley & Sons, 2011), p. 229-245.
- W. Sun, S. Nešić, R.C. Woollam, *Corros. Sci.* 51, 6 (2009): p. 1273-1276.
- J. Han, S. Nešić, Y. Yang, B. Brown, *Electrochim. Acta* 56, 15 (2011): p. 5396-5404.
- F. Madani Sani, B. Brown, Z. Belarbi, S. Nešić, "An Experimental Investigation on the Effect of Salt Concentration on Uniform CO₂ Corrosion," CORROSION 2019, paper no. 13026 (Houston, TX: NACE, 2019).
- F. Farelas, M. Galicia, B. Brown, S. Nešić, H. Castaneda, *Corros. Sci.* 52, 2 (2010): p. 509-517.
- J.L. Crolet, N. Thevenot, S. Nešić, *Corrosion* 54, 3 (1998): p. 194-203.
- C.A. Palacios, J.R. Shadley, *Corrosion* 47, 2 (1991): p. 122-127.
- S. leamsupapong, "Mechanisms of Iron Carbonate Formation on Mild Steel in Controlled Water Chemistry Conditions" (Ph.D. diss., Ohio University, 2016).
- M. Di Bonaventura, B. Brown, M. Singer, S. Nešić, "Effect of Flow and Steel Microstructure on the Formation of Iron Carbonate," CORROSION 2018, paper no. 11179 (Houston, TX: NACE, 2018).
- R. De Motte, R. Mingant, J. Kittel, F. Ropital, P. Combrade, S. Necib, V. Deydier, D. Crusset, *Electrochim. Acta* 290 (2018): p. 605-615.
- B. Ingham, M. Ko, G. Kear, P. Kappen, N. Laycock, J.A. Kimpton, D.E. Williams, *Corros. Sci.* 52, 9 (2010): p. 3052-3061.
- M. Ko, B. Ingham, N. Laycock, D.E. Williams, *Corros. Sci.* 80 (2014): p. 237-246.
- M. Ko, B. Ingham, N. Laycock, D.E. Williams, *Corros. Sci.* 90 (2015): p. 192-201.
- M.H. Sk, A.M. Abdullah, M. Ko, B. Ingham, N. Laycock, R. Arul, D.E. Williams, *Corros. Sci.* 126 (2017): p. 26-36.
- ASTM G1, "Standard Practice for Preparing, Cleaning, and Evaluating Corrosion Test" (West Conshohocken, PA: ASTM International, 2011).
- M. Singer, *Corrosion* 73, 8 (2017): p. 1030-1055.